Optimal operation of grid-connected hydropower plants through voltage control methods

Emil G. Melfald [a,*], Thomas Øyvang [a],

[a] *University of South-Eastern Norway, Department of Electrical Engineering, IT and Cybernetics, Campus Porsgrunn*
Emil.G.Melfald@usn.no
Thomas.Oyvang@usn.no

Abstract

The ongoing decarbonization, and the rapid increase in renewable penetration in the electric grid, will demand enhanced flexible operational schemes of the conventional hydropower plants. This paper explores a grid-connected hydropower plant's best-efficiency operating conditions when meeting the renewable energy transition. Power loss models combined with various voltage control methods are investigated for achieving optimal operation. This simulation study is carried out on a static Single Machine Infinite Bus (SMIB) environment to perform voltage control comparisons. Simulations show that the plant and grid power loss models can be utilized in an optimal controller setting to increase the accumulated average efficiency (AAE). However, optimal controllers had slow prediction times, and therefore a Reinforcement Learning (RL) method, A2C, has been trained to learn an optimal control policy that maximizes system efficiency. The RL agent supersedes the optimal control techniques with up to 40 times faster prediction times.

1 Introduction

In an energy mix with intermittent renewable energy sources such as wind and solar, the flexible operation of reliable reservoir-based hydropower plants can be the backbone for energy balance and increased stability (Pandey et al., 2021)(Abadie et al., 2020). Synchronous machines have inherent stability characteristics in the form of, e.g., rotational inertia and damper bars. Stability characteristics are further enhanced by controllers for frequency and voltage, e.g., the governor (GOV) and automatic voltage regulator (AVR) (*IEEE Recommended Practice for Excitation System Models for Power System Stability Studies*, 2016). Together they provide essential system services (constant frequency and voltage) for the operation of the electricity grid.

The Transmission System Operator (TSO) is responsible for the operational security of supply and power transfer capability while reducing investment costs and transmission losses (NVE, 2019). The active power dispatch is correlated to market demand by the TSO, while the voltage levels are considered more as free control variables in the power system operation. Through traditional centralized optimization techniques (Hasan et al., 2020), e.g., Optimal Power Flow (OPF) (Wang et al., 2017), grid losses and generation costs can be minimized with respect to active power production and terminal voltages (Qiu et al., 2009).

There has also been done much research on decentralized and distributed control schemes (Molzahn et al., 2017). This technique solves optimization problems by considering control of smaller grid sections instead of the complete system. Another approach for optimal control is reinforcement learning (RL). RL is a machine learning approach tailored to learning control policies to maximize an objective function, often referred to as a reward function (Buşoniu et al., 2018). Moreover, RL has been implemented in recent literature, e.g., for finding feasible grid voltage setpoints (Wang et al., 2020)(Duan et al., 2020), and energy management systems (Chen et al., 2021).

The use of power loss models of grid (Kundur, 1994) and synchronous machines (Bortoni et al., 2020) has the potential for more efficient voltage control.

This paper presents a simulation study comparing standard decentralized voltage control methods against optimal power system controllers. Controller schemes for efficiency maximization will be formulated and simulated in a grid-connected single machine infinite bus (SMIB) environment. Power losses are considered for the waterway, turbine, generator, and grid. Eight different controller methods under steady-state operation are considered. Four traditional primary setpoint control strategies of the AVR will be investigated. Three optimization-based controllers will be implemented and tested for the minimization of (i) generation losses, (ii) transmission losses, and (iii) overall losses. Finally, the A2C (Mnih and et al., 2016) reinforcement learning algorithm will be trained to maximize the system efficiency (plant and grid). The computational speed of RL compared to optimal controllers will be evaluated.

The paper is organized as follows. Section 2 introduces the power loss modeling for hydropower plants, while Section 3 introduces the different voltage controllers under study. Section 4 presents the study case and simulation results.

2 Power and energy loss modeling

In hydropower systems, the potential and kinetic energy in the water is converted first into mechanical energy before being converted to electrical energy. The electrical energy is then transported in cables, lines, and transformers,

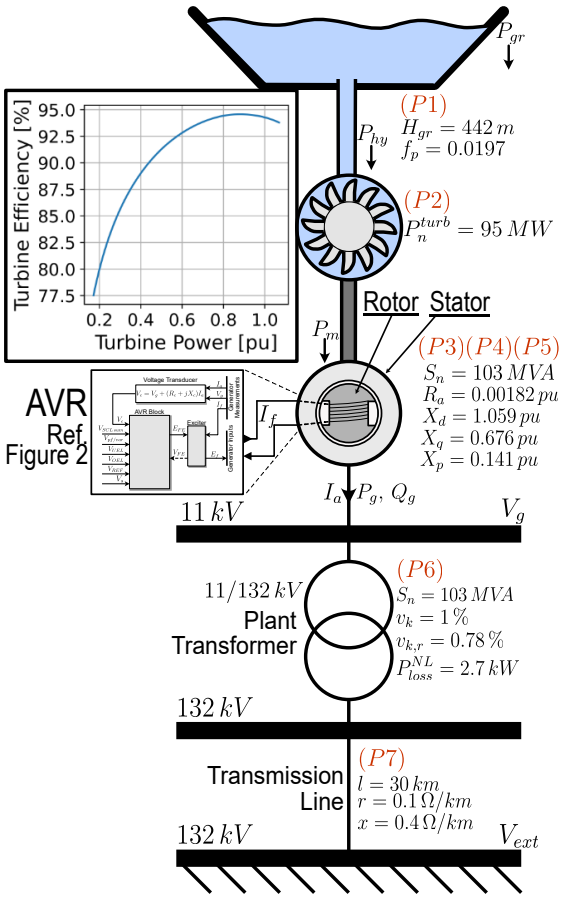

Figure 1: An overview of the SMIB topology and parameters. Power loss P1 to P7 are indicated close to the respective component.

which have some power losses. The power losses in a single machine infinite bus (SMIB) environment are proposed to be divided into seven different parts, e.g., (P1) to (P7). These losses are presented from top to bottom in Figure 1. The hydraulic losses (P1) represent water conduit friction losses from water movement. Turbine losses (P2) represent the power loss in the transition from pressure and kinetic energy to mechanical energy on the rotor shaft. The generator losses are divided into three separate categories: stator loss (P3), rotor loss (P4), and constant losses (P5). *Stator loss* (P3) is the ohmic losses $R_a I_a^2$ in the armature coils and stray loss. *Rotor loss* (P4) is the ohmic loss $R_f I_f^2$ from the field and excitation currents in the excitation circuit. *Constant losses* (P5) are friction and windage losses, core loss, and bearing losses. As long as the grid-connected machine's voltage and speed are constant, the constant losses will not change. Moreover, the transformer losses (P6) consist of constant and load-dependent losses. Finally, the transmission line losses (P7) are the ohmic losses in the transmission line. (Chapman, 2012)

2.1 *Synchronous generator loss modeling*

The calculation framework that was established in Bortoni et al. (Bortoni et al., 2020) is used for estimating the synchronous machine losses. This method extrapolates the machine losses by using known relations between armature current I_a, field current I_f, terminal voltage V_g, and nominal losses noted with *. *Stator loss* (P3) is extrapolated from nominal armature and stray losses, P_a^* and P_s^* respectively, as shown in Eq. 1. Armature current I_a should be known beforehand and is calculated from Eq. 2, implying that P_g, Q_g, and V_g are known.

$$P_{loss}^{stator} = (P_a^* + P_s^*)\left(\frac{I_a}{I_a^*}\right)^2 \tag{1}$$

$$I_a \angle -\varphi = \frac{P_g - jQ_g}{V_g} \tag{2}$$

Rotor loss (P4) is extrapolated from nominal field, brush, and excitation losses, P_f^*, P_{br}^*, and P_{ex}^* respectively, and depends on the field current I_f as shown in Eq. 3. For estimating the field current at any value of P_g, Q_g, and V_g, the generator's no-load and short-circuit characteristic curves are required. These curves are usually provided by the manufacturer or measured during commissioning of the machine. The no-load characteristics establish a relation between the internal emf E_g and field current I_f, usually linear. The short-circuit characteristics relates field and armature currents and capture saturation in the core. The saturation can be represented as the Potier reactance (X_p) and Potier emf (E_p) (Kundur, 1994). To calculate the field current I_f, the rotor angle δ and internal emf E_g is calculated with Eq. 4 (Kundur, 1994) and Eq. 5 (Chapman, 2012), respectively. The Potier voltage angle θ and emf E_p is calculated similarly through Eq. 6 and 7. Field current in the rotor circuit can then be estimated using Eq. 8. The parameters b_v, k, C_m, and m are obtained through curve fitting Eq. 8 to measured values of I_f in the short-circuit characteristic of the machine (Karikezi et al., 2021).

$$P_{loss}^{rotor} = (P_f^* + P_{br}^*)\left(\frac{I_f}{I_f^*}\right)^2 + P_{ex}^*\left(\frac{I_f}{I_f^*}\right) \tag{3}$$

$$\delta = \tan^{-1}\left(\frac{I_a(X_q\cos(\varphi) - R_a\sin(\varphi))}{V_g + I_a(X_q\sin(\varphi) + R_a\cos(\varphi))}\right) \tag{4}$$

$$E_g = V_g\cos(\delta) + I_a X_d\sin(\delta+\varphi) + R_a I_a\cos(\delta+\varphi) \tag{5}$$

$$\theta = \tan^{-1}\left(\frac{I_a(X_p\cos(\varphi) - R_a\sin(\varphi))}{V_g + I_a(X_p\sin(\varphi) + R_a\cos(\varphi))}\right) \tag{6}$$

$$E_p = V_g\cos(\theta) + I_a X_p\sin(\theta+\varphi) + R_a I_a\cos(\theta+\varphi) \tag{7}$$

$$I_f = \frac{E_g - E_p}{b_v} + k(E_p + C_m E_p^m) \tag{8}$$

Constant losses (P5) is extrapolated from the nominal core, bearing, friction and windage losses, noted P_c^*, P_b, and P_{wf}^*, respectively, where the core losses is dependent on the terminal voltage V_g, as shown in Eq. 9.

$$P_{loss}^{const} = P_c^*\left(\frac{V_g}{V_g^*}\right)^2 + P_b^* + P_{wf}^* \tag{9}$$

Nominal loss and saturation parameters for this paper's study case are displayed in Table 1 together with a short description of the parameters. The presented values are utilized for the study case calculations described in Section 4.

2.2 *Hydraulic and turbine loss modeling*

Hydraulic losses in the hydropower plant are separated into two parts, e.g., turbine losses and waterway losses, (P1) and (P2) in Figure 1 respectively. (P2) can be

Table 1: General Data for Loss Calculations of 103 MVA synchronous generator, turbine, and water way

Symbol	Description	Value
b_v	Saturation parameter	1.0 [.]
C_m	Saturation parameter	0.16 [.]
m	Saturation parameter	7 [.]
k	Saturation parameter	1.0308 [.]
I_a^*	Nominal Armature Current	5406.1 [A]
I_f^*	Nominal Field Current	1065 [A]
V_g^*	Nominal Generator Terminal Voltage	1 [pu]
P_a^*	Nominal Armature Losses	187.46 [kW]
P_s^*	Nominal Stray Losses	89.16 [kW]
P_f^*	Nominal Field Current Losses	173.65 [kW]
P_{br}^*	Nominal Brush Losses	2.13 [kW]
P_{ex}^*	Nominal Exciter Losses	15.88 [kW]
P_c^*	Nominal Core Losses	211.92 [kW]
P_b^*	Bearing Losses	240.9 [kW]
P_{wf}^*	Windage and Friction Losses	172.92 [kW]
q_w^*	Nominal Water Flow Rate	21.843 $[m^3/s]$
H_{gr}	Gross water head	442 [m]
f_p	Water way friction coefficient	0.0197 [.]

estimated from Eq. 10. The mechanical rotor power P_m is the generator output power P_g plus generator rotor, stator, and constant losses. The hydraulic power P_{hy} is the input power to the turbine before the conversion between kinetic/pressure water energy to mechanical energy and is calculated from Eq. 11.

$$P_{loss}^{turb} = P_{hy} - P_m = P_m \left(\frac{1}{\eta_{turb}} - 1 \right) \tag{10}$$

$$P_{hy} = \frac{P_m}{\eta_{turb}} \tag{11}$$

Calculating (P1) is done by solving Eq 12 concerning q_w. The gross power P_{gr} is the potential power from the water, assuming no losses, and is shown in Eq. 13. P_{loss}^H is estimated by the friction loss in the water way, shown in Eq. 14. ρ is water density in [kg/m^3], g is the acceleration of gravity in [m/s^2], H_{gr} is the gross water head in [m], H_{loss} is the head loss from friction [m], and q_w is the water flow rate [m^3/s]. Inserting Eq. 11, 13, and 14 into Eq. 12, yields a third degree polynomial for q_w, shown in Eq. 15. All values are known except for q_w, and this equation can therefore be solved. Assuming $q_w \in [0, q_w^*)$ only one solution to q_w is valid and used for the loss calculation.

$$P_{gr} = P_{loss}^H + P_{hy} \tag{12}$$

$$P_{gr} = \rho g H_{gr} q_w \tag{13}$$

$$P_{loss}^H = \rho g H_{loss} q_w = \rho g f_p q_w^3 \tag{14}$$

$$\rho g \left(H_{gr} q_w - f_p q_w^3 \right) - \frac{P_m}{\eta_{turb}} = 0 \tag{15}$$

2.3 Efficiency Calculations and AAE

The power loss calculation framework for the hydropower plant and transmission system has the following workflow. Firstly, the Active power P_g is defined. Then, the applied voltage controller determines the reactive power dispatch Q_g, and a power flow calculation is executed. The generator stator, rotor, and constant losses (P3, P4, P5) are calculated. Moreover, turbine loss (P2) and waterway loss (P1) are then calculated. From P_g and Q_g, the transformer loss P_{loss}^T (P6) and transmission loss P_{loss}^l (P7) are calculated through the Pandapowers power flow calculation (Thurner et al., 2018). For convenience, grid losses P_{loss}^{grid} and plant losses P_{loss}^{plant} is defined in Eq. 16 and 17, respectively.

$$P_{loss}^{grid} = P_{loss}^T + P_{loss}^l \tag{16}$$

$$P_{loss}^{plant} = P_{loss}^{stator} + P_{loss}^{rotor} + P_{loss}^{const} + P_{loss}^{turb} + P_{loss}^H \tag{17}$$

Overall system efficiency calculation is shown in Eq. 18. The numerator represents the active power reaching the external grid, while the denominator is the sum of active power production and losses from (P1) to (P7).

$$\eta = \frac{P_g - P_{loss}^{grid}}{P_g + P_{loss}^{grid} + P_{loss}^{plant}} \tag{18}$$

There are different ways of estimating the efficiency of a time series data set. One method is to average the efficiencies over the data. Another method proposed by (Karikezi et al., 2021) is the AAE (Accumulated Average Efficiency). In a data set of varying active power production, the AAE is a more accurate representation of the energy losses of the system compared to averaging over the efficiencies. Eq. 19 shows how AAE is calculated, assuming evenly spaced data points. The sum in the numerator represents the total energy production reaching the external grid (customers) in the data set. The sum in the denominator represents the total energy production and all losses.

$$\eta_{AAE} = \frac{\sum_{i=1}^{N} \left[P_g^{(i)} - P_{loss}^{grid(i)} \right]}{\sum_{i=1}^{N} \left[P_{loss}^{grid(i)} + P_{loss}^{plant(i)} + P_g^{(i)} \right]} \tag{19}$$

3 Voltage control methods

The rotor induces an internal emf $E_g \angle \delta$, determining the terminal voltage V_g and how much reactive power production/consumption the synchronous generator (SG) has. An approximate relation between the internal voltage and reactive power production is shown in Eq. 20 (Kundur, 1994).

$$Q_g = \frac{E_g^2 - E_g V_g \cos \delta}{X_d} \tag{20}$$

The excitation system of the SG, depicted in Figure 2 (*IEEE Recommended Practice for Excitation System Models for Power System Stability Studies*, 2016), determines both the terminal voltage and reactive power production. Transducers measure V_g, P_g, and Q_g on the generator terminal. These signals go through a voltage compensation block that calculates V_c. In this paper, the automatic voltage regulator AVR has two operating modes, indicated by switch SW1 and SW2 in the AVR block. If SW1 is closed, the AVR is in a voltage setpoint tracking mode. Two different controller modes are determined from this AVR state: constant voltage controller (C1) and voltage compensated controller (C2). Constant voltage control (C1) bypasses the voltage compensation block in Figure 2, effectively setting controller parameters R_c and X_c to 0. This mode controls the generator exciter such that $V_g = V_{REF}$, where V_{REF} is a voltage reference. Controller (C2) includes the voltage compensation block and is a setpoint controller that forces the resulting compensated voltage $V_c = V_{REF}$.

When SW2 is closed (and SW1 is open) the AVR is in reactive power setpoint mode. This AVR state can define

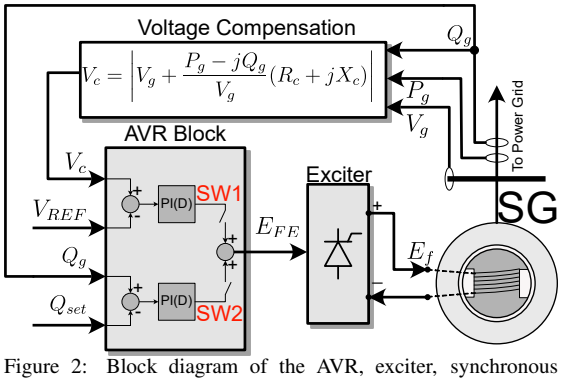

Figure 2: Block diagram of the AVR, exciter, synchronous machine, and voltage transducer (*IEEE Recommended Practice for Excitation System Models for Power System Stability Studies*, 2016).

two controller modes: constant Q_g controller (C3) and constant power factor controller (C4). Controller (C3) adjusts the excitation current such that the reactive power production reaches some setpoint value $Q_g = Q_{set}$. Controller (C4) updates Q_{set} continuously according to the active power production, such that $Q_{set} = P_g \tan \varphi_{set}$, where φ_{set} is the setpoint phase angle.
Controllers (C1) to (C4) are standard control modes for the AVR. No information on generator or grid losses is explicitly used in these controllers. Therefore, three optimal controllers and one RL controller are implemented, which produces optimal values of Q_{set} to the AVR, according to some objective function. The first optimal controller is an optimal plant efficiency control (C5) to minimize plant losses. The second optimal controller is the optimal grid efficiency (C6), which minimizes grid losses. The third optimal controller is an optimal system controller (C7), which minimizes the sum of plant and grid losses. In addition, a reinforcement learning (RL)-based controller (C8) is implemented to minimize system losses. All controllers, numbered (C1) to (C8) is listed in Table 2 with descriptions of controller objectives and tuned controller parameters.

3.1 Implementation of voltage controllers C1 to C7

Controller (C1) is equal to (C2), with the only difference being that parameters R_c and X_c are zero for (C1) and not for (C2). Therefore, the implementation for these two controllers is equal. In this paper, the generator bus is modeled as a PQ bus. This means P_g and Q_g have to be specified in the power flow calculation. Converting a voltage setpoint V_{REF} to a reactive power Q_g can be done through Eq. 21 - 23 and Algorithm 1.
The voltage V_c is adjusted towards a voltage setpoint V_{REF} and is calculated as the generator terminal voltage plus the voltage drop over a fictitious compensator impedance $Z_c = R_c + jX_c$ (*IEEE Recommended Practice for Excitation System Models for Power System Stability Studies*, 2016). The compensated voltage V_c is expressed in Eq. 21, where it is assumed that terminal voltage V_g has an angle of zero.

$$V_c \angle -\theta_c = V_g + \frac{1}{V_g}(P_g - jQ_g)(R_c + jX_c) \quad (21)$$

Separating Eq. 21 into real and imaginary parts results in Eq. 22 and 23. Assuming steady-state operation, V_c must be equal to the voltage reference, $V_c = V_{REF}$. Eq. 21 and 22 is a system of two equations with the two unknowns being the terminal voltage V_g and compensated voltage angle θ_c. Solving this system is done iteratively by using an initial power flow as a guess for V_g, which will be adjusted such that V_c converges to the reference voltage V_{REF}. Algorithm 1 shows this procedure.

$$V_g^2 - V_g V_c \cos(\theta_c) + P_g R_c + Q_g X_c = 0 \quad (22)$$

$$V_g V_c \sin(\theta_c) + P_g X_c - Q_g R_c = 0 \quad (23)$$

Table 2: Controller overview with a description of the controllers. Optimized controller parameters Θ^{opt} is displayed for controllers (C1) to (C4). Controller objectives are shown for optimal controllers (C5) to (C7), and the reward function $\mathcal{R}$ for the RL controller (C8).

Controller Name	Description	Tuned Controller Parameters/ Controller Objective
Const V (C1)	Setpoint control of V_g	$\Theta^{opt} \leftarrow V_{REF}$ = 1.02 pu
V-comp (C2)	Setpoint control of V_c	$\Theta^{opt} \leftarrow \begin{cases} V_{REF} = 1.00pu, \\ R_c = -0.03pu, \\ X_c = 0.043pu \end{cases}$
Const Q (C3)	Setpoint control of Q_g	$\Theta^{opt} \leftarrow Q_g^{set}$ = 7.01 Mvar
Const φ (C4)	Setpoint control of φ	$\Theta^{opt} \leftarrow \varphi$ = 0.002 rad
Opt Plant (C5)	Minimizes plant losses controlling Q_{set}	$Q_{set} = \min_{Q_{set}} \left(P_{loss}^{plant}\right)$
Opt Grid (C6)	Minimizes grid losses controlling Q_{set}	$Q_{set} = \min_{Q_{set}} \left(P_{loss}^{grid}\right)$
Opt Sys (C7)	Minimizes plant + grid losses controlling Q_{set}	$Q_{set} = \min_{Q_{set}} \left(P_{loss}^{grid} + P_{loss}^{plant}\right)$
RL control (C8)	RL control predicting Q_{set} for optimal system efficiency.	$\mathcal{R} = \left(\frac{P_g}{P_g + P_{loss}^{gen} + P_{loss}^{grid}}\right)^2$

Algorithm 1: Constant V controller (C2 and C4) at PQ bus.

Data: $Q_{set}^{(1)} = 0\,pu$, $Q_{set}^{(2)} = 0.1\,pu$
Do a power flow with $Q_{set}^{(1)}$ and $Q_{set}^{(2)}$ to obtain $V_c^{(1)}$ and $V_c^{(2)}$ by solving Eq. 22 and 23
while $|Q_{set}^{(2)} - Q_{set}^{(1)}| > 1\text{e}{-3}$ **do**
  $\frac{dQ_{set}}{dV_c} \leftarrow \frac{Q_{set}^{(2)} - Q_{set}^{(1)}}{V_c^{(2)} - V_c^{(1)}}$
  $Q_{set}^{new} \leftarrow Q_{set}^{(2)} + \frac{dQ_{set}}{dV_c}(V_{REF} - V_c^{(2)})$
  $V_c^{new} \leftarrow$ Power flow with $Q_g = Q_{g\,set}^{new}$
  $V_c^{(1)} \leftarrow V_c^{(2)}$, $V_c^{(2)} \leftarrow V_c^{new}$
  $Q_{set}^{(1)} \leftarrow Q_{set}^{(2)}$, $Q_{set}^{(2)} \leftarrow Q_{set}^{new}$
end
Result: Set $Q_{set} = Q_{set}^{(2)}$

Constant reactive power (C3) and constant power factor controller (C4) have, in essence, similar controller mechanisms, where a reactive power setpoint from the generator terminal Q_{set} is determined from the controllers and applied to the PQ bus directly.
The optimal controllers (C5, C6, and C7) utilize a minimization algorithm to achieve the controller objectives presented for each controller in Table 2. The

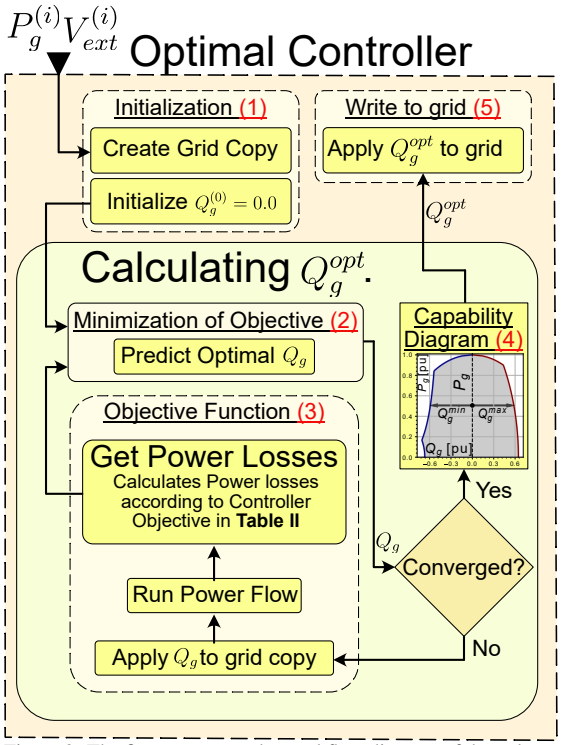

Figure 3: The figure presents the workflow diagram of the voltage controller C8 for calculating the optimal efficiency operation point Q_g^{opt} through step (1) to (4).

decision variable for the optimization is the reactive power setpoint Q_{set}.

The workflow diagram for the optimal controllers is illustrated in Figure 3, where the workflow steps are noted chronologically from step (1) to (5). The workflow diagram is explained in the sequel: In a time series simulation, an active power $P_g^{(i)}$ and external grid voltage $V_{ext}^{(i)}$ is given to the controller. The controller is initialized (1) by creating a grid copy, and the initial value for Q_g is specified at 0.0. A grid copy is made because the controller modifies the grid during the minimization of losses, and these modifications are not wanted in the original grid. The initial condition, a grid copy, and the objective function (3) is sent to the *minimize_scalar* function (2) from (Virtanen and et al., 2020), and utilizes the *brent* method. Step (2) and (3) is done iteratively to calculate an optimal value of Q_g^{opt}. When the minimization has converged, the optimal reactive power is bounded between a minimum and maximum allowed value, dictated by the capability diagram (4) (*IEEE Standard for Salient-Pole 50 Hz and 60 Hz Synchronous Generators and Generator/Motors for Hydraulic Turbine Applications Rated 5 MVA and Above*, 2006). The resulting reactive power value is then applied to the grid (5).

3.2 *Reinforcement Learning Controller C8*

Controller (C8) is a reactive power setpoint control based on the reinforcement learning method A2C (Mnih and et al., 2016). The utilized algorithm is implemented in StableBaselines 3 (Raffin et al., 2021), and the training environment for the agent is defined in the Gym framework (Brockman et al., 2016). The training environment is defined as a one-step deterministic environment, where the states $\mathcal{S} = \{V_{ext}, P_g\}$, and the action is $\mathcal{A} = \{Q_g\}$. During training, an episode is initialized by sampling state values P_g and V_{ext} from a uniform distribution, where $P_g\,[pu] \in [0.2, 1.0]$ and $V_{ext}\,[pu] \in [0.9, 1.1]$. The random sampling causes no two training episodes to be equal, and the agent should therefore learn to generalize for all allowed values of P_g and V_{ext}. Eq. 24 defines the reward function $\mathcal{R}$ that is utilized to find an optimal system control policy for Q_{set}.

$$\mathcal{R}(\mathcal{S}, \mathcal{A}) = \left(\frac{P_g}{P_g + P_{loss}^{gen} + P_{loss}^{grid}} \right)^2 \tag{24}$$

After a grid search, the highest resulting reward determined the A2C hyperparameters, with the results shown in Table 3. Hyperparameters not displayed in the table have default values from the SB3 library. Both the policy and value neural network sizes are relatively small and shallow. These small networks most likely caused faster training compared to larger networks. However, a higher learning rate of 0.1 did not yield improved results. The discount factor was not part of the search and was arbitrarily set to 1.0 as it doesn't affect the training in one-step environments.

Table 3: Tuned hyperparameters of the A2C Algorithm in SB3 on the Power System Loss Environment.

Hyperparameter	Value
Policy Neural Network Size	[8, 8]
Value Neural Network Size	[8, 8]
Steps before updating	32
Discount Factor γ	1.0
Learning Rate	0.01
Value function coefficient for the loss calculation	0.6

3.3 *Parameter tuning of controllers C1 to C4.*

As shown in Table 2, each controller (C1) to (C4) have different controller parameters noted as Θ. To find optimal parameter setting for each controller, parameters Θ is defined as a decision variable in an optimization problem, as shown in Eq. 25. The objective function is to minimize overall system power losses for each controller as shown in Eq. 26. The system losses is defined in Eq. 27. Nine operating points close to the nominal (rated) operation is used in the objective function to achieve optimal controller parameters Θ_{opt}. Three values of external grid voltage is chosen, where $V_{ext}\,[pu] = \{0.99, 1.0, 1.01\}$, For each external grid voltage level, three active power levels are chosen, where $P_g\,[pu] = \{0.9, 0.95, 1.0\}$. These operating points is represented as the two summations in Eq. 26. The optimization results of Θ for each controller is shown in Table 2 as Θ^{opt}.

$$\Theta_{opt} = \min_{\Theta} J(\Theta) \tag{25}$$

$$J(\Theta) = \sum_{i=1}^{3} \sum_{j=1}^{3} \left[P_{loss}(P_g^{(i)}, V_{ext}^{(j)}; \Theta) \right] \tag{26}$$

$$P_{loss}(P_g^{(i)}, V_{ext}^{(j)}; \Theta) = P_{loss}^{plant} + P_{loss}^{grid} \tag{27}$$

4 Simulation results of a 103 MVA study case

A SMIB (Single Machine Infinite Bus) testbed with the presented controllers was established on a grid-connected 103 MVA hydro generator. The system overview is shown in Figure 1, and system parameters are listed in Table 1.

4.1 *Controller efficiency characteristics*

Figure **??**hows the controller efficiency characteristics for a range of active power and external voltage values for all controllers. Efficiencies are estimated by Eq. 18 for a range of external voltage (x-axis) and active power (y-axis) combinations. The P_g and V_{ext} axis each has 30 evenly spaced data points on which the contours are based. A reactive power dispatch is calculated from the voltage controllers at each point, followed by a power flow and efficiency calculation. In addition, the yellow "x" in each subplot in Figure 4 indicates the Best Efficiency Point (BEP). BEP is the point where the values of P_g and V_{ext} yield the highest system efficiency for a given controller. Moreover, the efficiency value for each BEP is shown in Table 4.

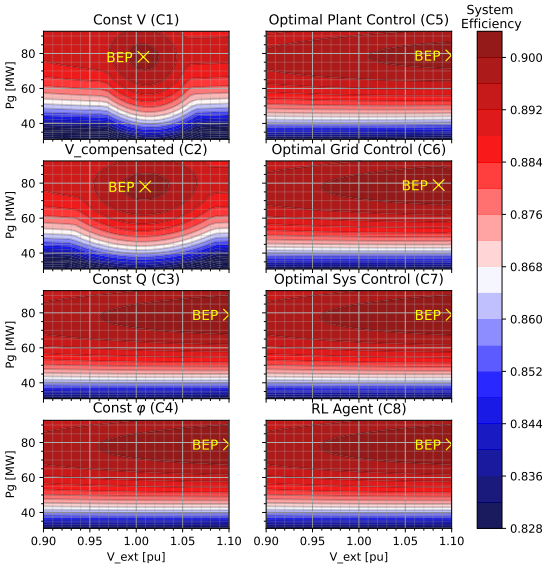

Figure 4: Efficiency characteristic plots for the eight presented controllers. Moreover, the BEP point for each controller is highlighted.

4.2 *Controller performance indicators and data set*

Controller performance is evaluated through two indicators. These are i) the energy losses in the grid, plant, and system and ii) the voltage variation at the generator bus. These indicators will be evaluated by simulating the SMIB environment with an artificially made data set, which is displayed in Figure 5. In total, there are 8760 values of P_g and V_{ext}. The data set is available in (Melfald, n.d.), and was generated by sampling the active power and external voltage values from normal distributions. When making the data set, the average active power value was set to 0.7 pu with a standard deviation of 0.3, $P_g \sim \mathcal{N}(0.7, 0.3^2)$. Sampled values was bounded between 0.3 and 0.9, such that $P_g \in [0.3, 0.9]$. The average external voltage value was set to 1.0 pu with a standard deviation of 0.02 with no bounds, $V_{ext} \sim \mathcal{N}(1.0, 0.02^2)$. It is assumed to be a one-hour time-step per data point.

4.3 *Energy losses and efficiencies from simulation*

The energy losses, and terminal generator voltage, are obtained from the simulation of the 8760 data points. Results from the simulation are shown in Table 4. The grid, plant, and system losses are calculated from accumulated power losses. A system

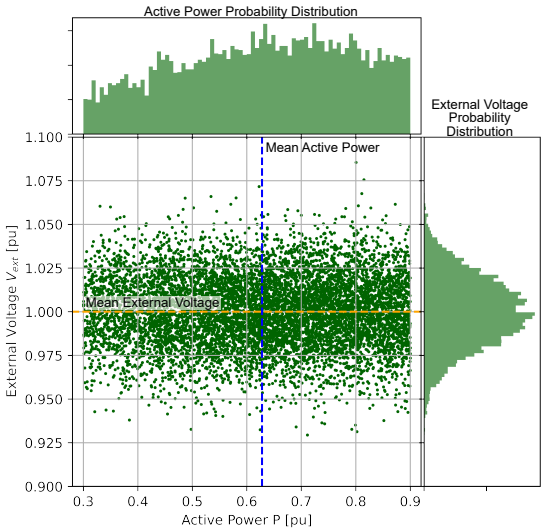

Figure 5: Data Points used for efficiency comparison between voltage controllers. (Melfald, n.d.)

energy loss comparison is made with ΔP_{add}^{sys}. This variable is obtained by subtracting the system losses of any controller with the system losses of controller (C7). This represents additional system losses generated by not utilizing controller (C7). Similarly, the additional grid losses ΔP_{add}^{grid} is comparing the grid losses when using (C6) against the other controllers. Additional plant losses ΔP_{add}^{plant} are also compared between controller (C5) and the rest of the controllers.

4.4 *Voltage variation comparisons*

The voltage variation on the generator terminal V_g for different controllers is shown and compared in the box plot in Figure 6 (a). The box plot shows four properties of the voltage variation in the study case for each controller. First, the green horizontal line in each box represents the median value of the voltages. The box's upper and lower vertical boundaries represent the middle 50 percent of the voltage points, assuming a sorted data set. There is no box for (C1) because the voltage variation is negligible for large parts of the data set. The lines stretching out vertically from the boxes are called "whiskers" and show the boundaries between the data and outliers, represented as small circles outside the whiskers. The lower outliers are defined as data points with voltage values lower than 0.01 % of the data set. Upper outlier data points are values above 99.9 % of the data set. In addition, arrows to the left of all boxes and whiskers are displayed with a number. The arrows and number represent the maximum voltage variation [%] in the positive and negative direction from the median voltage in the simulation.
The voltage variation in Figure 6 (a) shows that controllers (C3, C4, C6, C7, C8) have similar generator voltage variation throughout the simulation. This similarity indicates that the reactive power dispatch is similar for the controllers, which is shown with the reactive power distributions in Figure 6 (b). On average, the optimal plant controller (C5) has lower terminal voltage values during the simulation. The main reason for this is that the optimal plant operation for the generator is close to 0.2 reactive power consumption, as described by (Karikezi et al., 2021). This reactive power consumption lowers the terminal voltage compared to the other controllers with a higher reactive power dispatch.

Table 4: Result Data from power flow simulations of the 8760 data points.

	Const V C1	V-comp C2	Const Q C3	Const φ C4	Opt Plant C5	Opt Grid C6	Opt Sys C7	RL Agent C8
AAE [%]	87.6	87.812	87.914	87.936	87.754	87.932	87.937	87.936
Total System Losses [MWh]	70251	69048	68469	68346	69377	68371	68341	68346
Total Grid Losses [MWh]	10925	9983	9410	9405	10614	9378	9404	9394
Total Plant Losses [MWh]	59326	59064	59058	58941	58762	58992	58937	58951
ΔP_{add}^{sys} [MWh]	1910.3	706.5	127.5	5.1	1035.7	29.6	0.0	4.5
ΔP_{add}^{grid} [MWh]	1547.1	605.5	32.4	26.8	1236.1	0.0	25.8	16.1
ΔP_{add}^{plant} [MWh]	563.7	301.5	295.6	178.8	0.0	230.1	174.6	188.9
BEP Efficiency [%]	90.134	90.135	90.309	90.324	90.144	90.300	90.325	90.324
Calculation Speed [steps/s]	12.9	12.7	25.5	32.1	5.6	1.3	0.8	34.2

The constant voltage controllers (C1, C2) have the lowest voltage variation and, consequently, the highest reactive power variation. When the external grid voltage V_{ext} changes, controller (C1) and (C2) force the terminal voltage towards the voltage setpoint by adjusting the reactive power dispatch. The reactive power dispatch is proportional to the voltage difference between V_{ext} and controller voltage setpoint V_{REF}. It is therefore clear from Figure 6 (c) that controllers (C1) and (C2) operate less efficiently compared to the other controllers.

5 Discussion

Figure 4 shows that the active power has the most significant impact on the system efficiency, with Best Efficiency Points (BEPs) residing at around 80 MW for all controllers. However, there is a significant difference between the BEPs on the V_{ext} axis. All controllers except (C1) and (C2) prefer higher V_{ext}, likely because of the lower currents leading to lower ohmic losses.

Controller (C1) and (C2) have, on average, higher reactive power dispatch because of the additional reactive compensation needed for constant voltage control, indicated in Figure 6 (a) and (b). Therefore, the BEPs of these controllers reside where V_{ext} is close to V_{REF}. With similar generator and external voltage values, the reactive power dispatch is close to 0. Lower reactive power flow has higher efficiencies according to Figure 6 (c).

The additional system losses ΔP_{add}^{sys} in Table 4 indicates that the optimal grid controller (C6) has almost the same performance as the system-wide optimal control (C7). This indicates that the grid is most sensitive to the reactive power flow. The optimal plant control (C5) is overall inefficient. An explanation for this is that the reactive power dispatch of around -0.2 pu, which negatively affects the grid efficiency. The saved losses in the plant are less than the additional grid losses at this reactive power dispatch level, which is clear from the efficiency curves in Figure 6 (c).

Both constant voltage controllers (C1 and C2) have the lowest voltage deviation but at the cost of lower AAE compared to the other controllers. The constant V control (C1) has the best performance for limiting the voltage variation and the worst efficiency. The compensated V controller (C2) showed some efficiency improvements, but at the cost of having a higher voltage variation.

Table 4 also shows that the difference between the optimal system controller (C7) and RL controller (C8) is relatively small, indicating that the RL agent learned an approximate optimal control policy. The main difference between (C7) and (C8) is the calculation speed. The RL agent is a factor about 40 times faster than (C7). Such a prediction speed is achieved because the RL agent does not require an iterative solver to predict Q_g, and predicts Q_g directly based on the system states P_g and V_{ext}.

6 Conclusions

This paper has studied eight different voltage control methods for the best efficiency operation of a grid-connected hydropower plant. The results are promising and show that improved efficiency for the overall system, plant, and grid efficiency is available as more knowledge on the power losses of the system is provided. Moreover, results indicate that overall system efficiency increases for both the optimal controllers (C5) and (C7), and the RL controller (C8) compared to the traditional control methods (C1-C4). Combining a hydropower plant loss model with traditional optimal power flow methods on the grid side improves the accumulated average efficiency (AAE) by reducing total power losses and increasing revenue for plant owners and TSOs. The RL algorithm A2C has shown to be capable of learning an approximate optimal system control policy for maximizing system efficiency. The main difference between (C7) and (C8) is that (C8) has a significantly faster computational time. RL can therefore be considered viable for online operation with time frames of seconds. However, simulations show that voltage variation on the generator bus is higher when utilizing controllers for increased system efficiency compared to voltage setpoint controllers (C1) and (C2).

Future work should focus on expanding the power system size. In addition, voltage restrictions as part of the reward/objective functions should be implemented. Moreover, an in-depth dynamic studies on system stability criteria must be implemented in further studies.

Acknowledgment

We gratefully acknowledge the support from The Research Council of Norway and industry partners through Research Council project “ref: 326673” (SysOpt).

References

Abadie, L. M., Chamorro, J. M., Huclin, S. and van de Ven, D. J. (2020), ‘On flexible hydropower and security of supply: Spain beyond 2020’, *Energy* **203**, 117869. doi: 10.1016/J.ENERGY.2020.117869.

Bortoni, E. C., Uemori, M. K. I., Araujo, B. T., Bernardes, J. V., Rocha E., J. J. and Siniscalchi, R. T. (2020), Accurate methodology to obtain efficiency mapping of synchronous machines, *in* ‘2020 IEEE Power Energy Society General Meeting (PESGM)’, pp. 1–5. doi: 10.1109/PESGM41954.2020.9281622.

Brockman, G., Cheung, V., Pettersson, L., Schneider, J., Schulman, J., Tang, J. and Zaremba, W. (2016), ‘Openai gym’.

Buşoniu, L., de Bruin, T., Tolić, D., Kober, J. and Palunko, I. (2018), ‘Reinforcement learning for control: Performance,

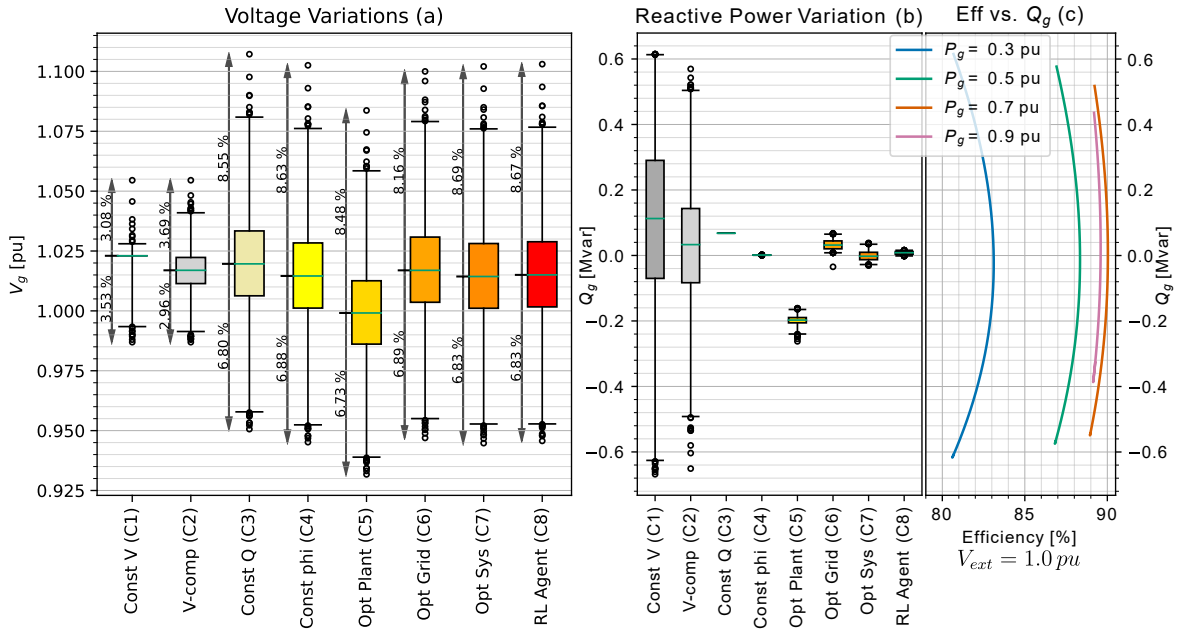

Figure 6: Fig. (a) shows the voltage variation Box & Whiskers plot from simulation of the 8760 data points in the study case, with indications of the % variation from the median value. Fig. (b) shows the reactive power dispatch distributions for the controllers and corresponds to the voltage variation distributions. Fig. (c) illustrates the system efficiency over reactive power values for four different active power levels, namely $P_g = 0.3$, 0.5, 0.7, and 0.9 pu. The external grid voltage is set to 1.0 pu for the shown efficiency curves.

stability, and deep approximators', *Annual Reviews in Control* **46**, 8–28. doi: 10.1016/J.ARCONTROL.2018.09.005.

Chapman, S. J. (2012), *Electric Machinery Fundamentals*, 5 edn, New York: McGraw-Hill.

Chen, Y., Peng, X., Xu, X. and Wu, H. (2021), 'Deep Reinforcement Learning based Applications in Smart Power Systems', *Journal of Physics: Conference Series* **1881**(2), 361–371. doi: 10.1088/1742-6596/1881/2/022051.

Duan, J., Shi, D., Diao, R., Li, H., Wang, Z., Zhang, B., Bian, D. and Yi, Z. (2020), 'Deep-Reinforcement-Learning-Based Autonomous Voltage Control for Power Grid Operations', *IEEE Transactions on Power Systems* **35**(1), 814–817. doi: 10.1109/TPWRS.2019.2941134.

Hasan, F., Kargarian, A. and Mohammadi, A. (2020), *A Survey on Applications of Machine Learning for Optimal Power Flow*. doi: 10.1109/TPEC48276.2020.9042547.

IEEE Recommended Practice for Excitation System Models for Power System Stability Studies (2016), *IEEE Std 421.5-2016 (Revision of IEEE Std 421.5-2005)* pp. 1–207. doi: 10.1109/IEEESTD.2016.7553421.

IEEE Standard for Salient-Pole 50 Hz and 60 Hz Synchronous Generators and Generator/Motors for Hydraulic Turbine Applications Rated 5 MVA and Above (2006), *IEEE Std C50.12-2005 (Previously designated as ANSI C50.12-1982)* pp. 1–45. doi: 10.1109/IEEESTD.2006.99082.

Karikezi, Y. C., Nøland, J. K. and Øyvang, T. (2021), 'The Energy Transition ' s Impact on the Accumulated Average Efficiency of Large Hydrogenerators', *IEEE Transactions on Energy Conversion* pp. 1–10.

Kundur, P. (1994), *Power system stability and control*, New York : McGraw-Hill.

Melfald, E. G. (n.d.), 'Opensimhub/sysopt-wp1-hydropowercontrol: 2022-09-sims2022 (2022-09-sims2022)'. doi: 10.5281/zenodo.6597305.
URL: *https://doi.org/10.5281/zenodo.6597305*

Mnih, V. and et al. (2016), 'Asynchronous methods for deep reinforcement learning'. doi: 10.48550/ARXIV.1602.01783.

Molzahn, D. K., Dörfler, F., Sandberg, H., Low, S. H., Chakrabarti, S., Baldick, R. and Lavaei, J. (2017), 'A survey of distributed optimization and control algorithms for electric power systems', *IEEE Transactions on Smart Grid* **8**(6), 2941–2962. doi: 10.1109/TSG.2017.2720471.

NVE (2019), 'System operation in the Norwegian power system'.
URL: *https://2021.nve.no/norwegian-energy-regulatory-authority/system-operation-in-the-norwegian-power-system/*

Pandey, M., Winkler, D., Sharma, R. and Lie, B. (2021), 'Using mpc to balance intermittent wind and solar power with hydro power in microgrids', *Energies* **14**(4). doi: 10.3390/en14040874.

Qiu, Z., Deconinck, G. and Belmans, R. (2009), A literature survey of optimal power flow problems in the electricity market context, *in* '2009 IEEE/PES Power Systems Conference and Exposition', pp. 1–6. doi: 10.1109/PSCE.2009.4840099.

Raffin, A., Hill, A., Gleave, A., Kanervisto, A., Ernestus, M. and Dormann, N. (2021), 'Stable-baselines3: Reliable reinforcement learning implementations', *Journal of Machine Learning Research* **22**(268), 1–8.
URL: *http://jmlr.org/papers/v22/20-1364.html*

Thurner, L., Scheidler, A., Schäfer, F., Menke, J., Dollichon, J., Meier, F., Meinecke, S. and Braun, M. (2018), 'pandapower — an open-source python tool for convenient modeling, analysis, and optimization of electric power systems', *IEEE Transactions on Power Systems* **33**(6), 6510–6521. doi: 10.1109/TPWRS.2018.2829021.

Virtanen, P. and et al. (2020), 'SciPy 1.0: Fundamental Algorithms for Scientific Computing in Python', *Nature Methods* **17**, 261–272. doi: 10.1038/s41592-019-0686-2.

Wang, S., Duan, J., Shi, D., Xu, C., Li, H., Diao, R. and Wang, Z. (2020), 'A Data-Driven Multi-Agent Autonomous Voltage Control Framework Using Deep Reinforcement Learning', *IEEE Transactions on Power Systems* **35**(6), 4644–4654. doi: 10.1109/TPWRS.2020.2990179.

Wang, Y., Wang, S. and Wu, L. (2017), 'Distributed optimization approaches for emerging power systems operation: A review', *Electric Power Systems Research* **144**, 127–135. doi: 10.1016/J.EPSR.2016.11.025.